ELSEVIER

Journal of Power Sources 89 (2000) 40–45

JOURNAL OF POWER SOURCES

www.elsevier.com/locate/jpowsour

Structural stability of aluminum stabilized alpha nickel hydroxide as a positive electrode material for alkaline secondary batteries

Jinxiang Dai [a], Sam F.Y. Li [a,b,*], T. Danny Xiao [c], Donald M. Wang [c], David E. Reisner [c]

[a] *Department of Chemistry, National University of Singapore, 10 Kent Ridge Crescent 119260, Singapore*
[b] *Institute of Material Research and Engineering, National University of Singapore, 10 Kent Ridge Crescent, 119260, Singapore*
[c] *US Nanocorp, Inc., 20 Washington Avenue, North Haven, CT 06437, USA*

Received 29 October 1999; accepted 27 December 1999

Abstract

Nanostructured, aluminum-stabilized nickel, hydroxides described as $Ni_{1-x}Al_x(OH)_2.(CO_3)_{x/2} \cdot nH_2O$ ($x = 0.05–0.2$), which are similar to α-$Ni(OH)_2 \cdot xH_2O$ in crystal structure are examined as cathode materials for Ni–Cd cells. The structure, morphology and electrochemical performance are investigated. The structural changes and stability of nanophase aluminum-stabilized, alpha nickel hydroxides with different x values analyzed during cycling by means of powder X-ray diffraction. Compared with β-$Ni(OH)_2$, the nanophase, aluminum-stabilized α-$Ni(OH)_2$ with $x = 0.15$ is highly stable against overcharge.

Keywords: Alpha nickel hydroxide; Secondary battery

1. Introduction

Nickel hydroxide electrode, $Ni(OH)_2/NiOOH$, has been used as a positive (cathode) electrode in commercial alkaline secondary batteries for more than 100 years [1]. To date, it is still one of the best electrodes for these batteries. The major battery systems Ni–Cd and Ni–MH, are widely used in Walkman, compact disc, and cassette players, camcorder, notebook computers, and electric vehicles.

The complex electrochemical reaction schemes of nickel hydroxide in nickel electrodes have been thoroughly studied [2,3], but are not yet completely understood. During the charge–discharge, the electrochemical mechanism, which was first elucidated by Bode et al. [4], may be described as follows:

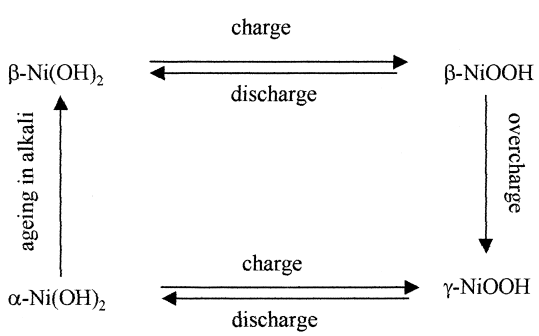

The β-$Ni(OH)_2$ crystallizes with a hexagonal brucite structure with an inter-sheet distance of 4.6 Å [5]. β-$Ni(OH)_2$ is often selected as a discharged-state active

* Corresponding author. Tel.: +65-874-2681; fax: +65-779-1691.
E-mail address: chmlifys@nus.edu.sg (S.F. Li).

0378-7753/00/$ - see front matter
PII: S0378-7753(00)00391-8

material in the preparation of nickel electrodes because: (i) it is stable in strong alkaline electrolyte and has good reversibility when charged to β-NiOOH; (ii) β-NiOOH has a similar structure with a lattice constant of inter-sheet 4.85 Å. Only 0.8 electron capacity is available in β–β conversion, because the average Ni oxidation state of β-$Ni(OH)_2$ produced under mild electrochemical oxidation is lower than 2.8 [6]. Higher capacity charging under strong electrochemical oxidation may result in the over-charged product, γ-NiOOH, which contains Ni^{4+} and has a larger lattice constant of about 7 Å [6,7]. The conversion of β-$Ni(OH)_2$ to γ-NiOOH is accompanied by a large volumetric change and this may result in loss of contact between the active material and the conductive ingredients, thus causing fast capacity fading during charge–discharge cycling. Therefore, overcharge of the electrode is always avoided in battery applications.

α-$Ni(OH)_2$ is highly hydrated and can be represented by the formula $3Ni(OH)_2 \cdot [2H_2O]$. It consists of a sandwich-type structure with a plane of Ni atoms between an array of O atoms. Between each nickel–oxygen sandwich, there is a disordered layer of intercalated water molecules. α-$Ni(OH)_2$ is oxidized to hydrous γ-NiOOH. The lattice constants of α-$Ni(OH)_2$ and γ-NiOOH are nearly identical, ~7. Thus, the α–γ conversion with α-$Ni(OH)_2$ as the primary material is likely to be suitable for battery application. It is widely realized that γ-$Ni(OH)_2$ contains some quadrivalent (Ni^{4+}) nickel as well as trivalent nickel to yield average oxidation states of 3.5 or higher. $K(NiO_2)_3 \cdot xH_2O$, which has a valency of 3.67 has been proposed [4,8]. As suggested by Corrigan and Knight [8], however, the higher oxidation state does not necessarily translate into more than one electron capacity, because the real oxidation state change of nickel in the α–γ system may be from + 2.5 to + 3.5. On the other hand, α-$Ni(OH)_2$ reverts to β-$Ni(OH)_2$ on storage in strong alkali [4,9]. α-$Ni(OH)_2$ synthesized by reaction of NH_3 with $Ni(NO_3)_2$ shows a high capacity of 420 mA h g^{-1} in a cell, but decreases rapidly when cycled between the charged and the discharged state because of conversion to the β structure [10]. The α–γ conversion continues to be pursued because of the possibility to obtain more than one electron capacity. A type of alpha nickel hydroxide in which 30% nickel, was substituted by cobalt showed 1.1 electron conversion during charge and discharge cycle cycling [11]. Kamath et al. [12], demonstrated the use of aluminum to stabilize the structure of α-$Ni(OH)_2$. Recently, a type of α-$Ni(OH)_2$ with 25 mol% Ni substituted by Zn was studied [13]. Overall, these findings show that, stabilized α-$Ni(OH)_2$ is stable on storage in strong alkali and provide a higher specific capacity than β-$Ni(OH)_2$. On the other hand stability against extensive cycling and overcharging has not been confirmed.

The purpose of the present study is to investigate the structure stability of nanostructured, aluminum-stabilized $Ni(OH)_2$ against prolonged cycling, and overcharging.

2. Experimental

2.1. Preparation of active materials

Nanophase, aluminum stabilized, α-$Ni(OH)_2$ was synthesized via a wet chemical synthesis technique. The detailed synthesis procedure has been reported elsewhere [16]. Similar to Reichle's synthesis [14,15], the as-synthesized nanophase α-nickel hydroxide has a $Ni_{1-x}Al_x(OH)_2.(CO_2)_{x/2} \cdot nH_2O$ crystal structure. The active material, after material process treatment, has a taping density of 1.6 g cm^{-3}. Two types of high-density $Ni(OH)_2$ were used as reference materials: (i) Japanese Tanaka spherical β-$Ni(OH)_2$; (ii) US Nanocorp's nanophase spherical β-$Ni(OH)_2$. Both varieties have a taping density of 2.0 to 2.1 g cm^{-3}. In experiments, it was that the materials displayed no significant differences. Both of them are termed as 'high density spherical β-$Ni(OH)_2$'. The structures of the nickel hydroxides used in the experiments were analyzed by a Philips X-ray diffractrometer with CuKα1 (λ = 1.54056Å).

2.2. Electrochemical test

Positive electrodes were made by pasting a slurry mixture of $Ni(OH)_2$, nickel powder (graphite powder, KS-44), carboxymethylcellulose (CMC) and Teflon in water on nickel discs. The area of the nickel disc was 3.14 cm^2. After pasting, the electrodes were dried in an oven at 100°C for 6 h. The weight composition of the composite positive material was: $Ni(OH)_2$ — 76%; nickel powder 20% (or graphite 10%); CMC — 2%; Teflon — 2%. Two kinds of conductive additives were used, alternatively, for identifying the diffraction peaks of the active material after cycling because the diffraction peaks of graphite or nickel might interfere with the identification of the diffraction peaks of the active materials. In the present experiments, we found that the slight differences in the two conductive additives were found not to affect the electrochemical performance of the cells. The negative electrode was $Cd/Cd(OH)_2$, as used in commercial Ni–Cd batteries. Test at a constant current discharge of 9.4 mA and cycle performance were performed with an UBAIII Vencon battery analyzer. In the cycle test, the cells were charged to 1.6 to 1.8 the capacity of the first discharge with a current of 4.0 mA. The cycle conditions of the cells with different materials were not completely identical because of the different mass and specific capacity. In the experiment, the charge current densities of different cells were maintained as about 60 mA g^{-1}. It was found that the discharge current density, over a range of 130 to 210 mA g^{-1}, had no significant effect on cycle performance. All cells were tested at room temperature. The electrolyte was 32 wt.%. KOH solution with 2 wt.% LiOH.

3. Results and discussions

3.1. Structure and phase determination

The XRD patterns for nanophase $Ni(OH)_2$ with different aluminum concentrations (5 to 20 mol%), are presented in Fig. 1(B–E). The XRD pattern for high-density spherical β-$Ni(OH)_2$ is plotted in Fig. 1(A). The distinction between the α and β-phase $Ni(OH)_2$ is the location of the lowest 2θ diffraction peaks. As can be seen from Fig. 1, 001 diffraction occurs at $2\theta = 19.228°$ and corresponds to an inter-sheet distance of 4.6122 Å for the β-$Ni(OH)_2$, while the lowest 2θ diffraction occurs at $2\theta = 11.152°$, $d = 7.927$ for 15 wt.% Al α-$Ni(OH)_2$ and at $2\theta = 11.342°$, $d = 7.795$ for 20 wt.% Al α-$Ni(OH)_2$.

Without aluminum, the as-synthesized $Ni(OH)_2$ has an β-type crystal structure. At 5-mol% aluminum concentration, a small peak appears at $2\theta \sim 11°$. This indicates the presence of a small concentration of α-$Ni(OH)_2$. A broad peak at 19.626° and a narrow peak at 33.434° show it contains a β phase. Increasing the Al concentration from 5 to 20 mol%, increases the intensity of $2\theta \sim 11°$ diffraction. At 20 mol% Al, full transformation to the α phase occurs. The results partly agree with those reported previously [12]. It is concluded that both the 10 and 15 wt.% Al samples contain β phase. This may be the reason why they could not be well indexed by Kamath et al. [12].

3.2. Electrochemical performance analysis

The cell cycle performance of cells with different cathode materials is shown in Fig. 2. The cathode material

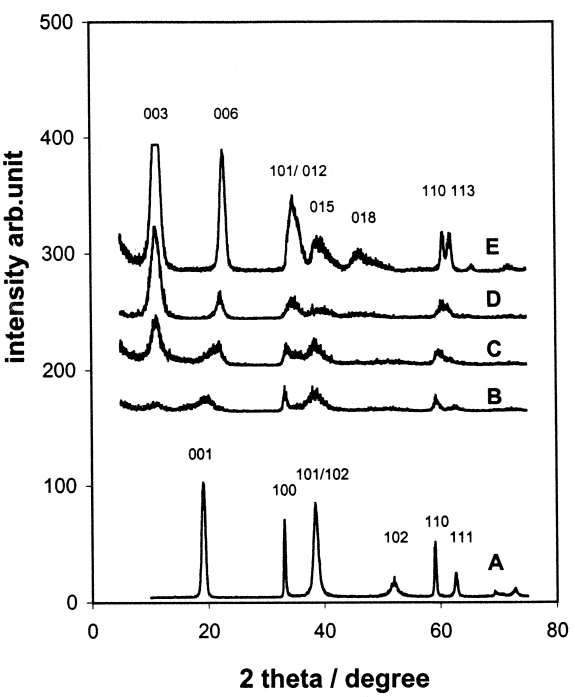

Fig. 1. XRD patterns for different nickel hydroxides. (A) high-density spherical β nickel hydroxide; (B) 5 mol% Al–$Ni(OH)_2$; (C) 10 mol% Al–$Ni(OH)_2$; (D) 15 mol% Al–$Ni(OH)_2$; (E): 15 mol% Al–$Ni(OH)_2$.

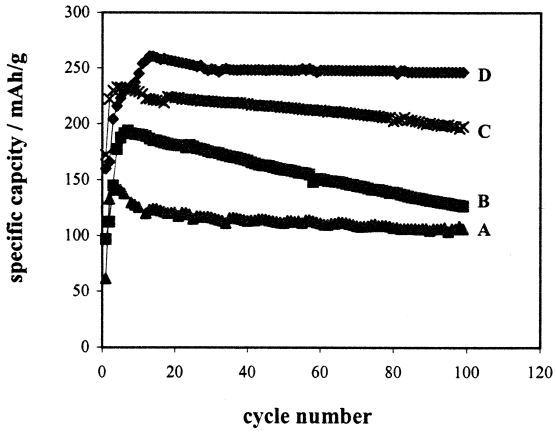

Fig. 2. Cycling performance of cells with different nickel hydroxides, discharged to 0.9 V. (A) 5 mol% Al–$Ni(OH)_2$, discharge 209 mA g^{-1}, charge 59.3 mA g^{-1}, 4.5 h; (B) 10 mol% Al–$Ni(OH)_2$, discharge 159.3 mA g^{-1}, charge 67.8 mA g^{-1} 4.5 h; (C) high-density spherical β nickel hydroxide, discharge 149 mA g^{-1}, charge 63.5 mA g^{-1} 5.8 h; (D) 15 mol% Al–$Ni(OH)_2$, discharge 136 mA g^{-1}, charge 58.0 mA g^{-1} 7 h.

with 15 mol% Al (curve *D*) has the best specific capacity and stability. Its highest specific capacity is 260 mA h g^{-1}, which corresponds to 1.0 electron transfer according to the formula $Ni_{1-x}Al_x(OH)_2.(CO_3)_{x/2} \cdot 0.66H_2O$ ($x = 0.15$). The high density spherical nickel hydroxides (curve *C*) show lower specific capacities and their highest capacity is about 230 mA h g^{-1}, which corresponds to 0.8 electron transfer. More electron transfer per Ni is characteristic of α–γ conversation because Ni^{4+} can exist in γ-$Ni(OH)_2$ [4,8]. The structure of the charged and the overcharged states will be discussed later. Many researchers have found [17] that the oxidation state of an anode oxidized, pure β phase is 2.7 rather than the expected 3.0. Barnard et al. [18] also found that it was difficult to achieve a pure β-NiOOH phase by anodic oxidation (charging) in concentrated alkali [18]. Upon overcharging, γ-NiOOH can be produced and it may be reduced to a type of β phase (termed $\beta_{ex\,\gamma}$), which is similar to γ-NiOOH [19]. The available capacity is, however, still limited to ~0.8 electron per formula because the working voltage of γ–$\beta_{ex\,\gamma}$ is only 0.8 V [19]. By the contrast, the α–γ system does not have this limitation and may give out 1 or more electron transfer.

The nickel hydroxide containing 10-mol% Al (curve *B*) has a lower specific capacity than that of high density spherical nickel hydroxide, and is less stable and fades faster during charge–discharge cycling. 5 mol% Al–$Ni(OH)_2$ (curve *A*) exhibits the lowest specific capacity. The lower specific capacity and inferior stability of 5 and 10 mol% Al samples may be caused by structure fading in KOH electrolyte or fading with charge–discharge cycling. The fading of the crystal structure may result in crystallite breaking and loss of contact of the active materials with the conductive substrate. The structural change will be discussed later.

In order to elucidate further the charge–discharge stability and discharge characteristics of different cathode materials, a study, was made of the discharge curves of cells with different cathode materials. From Fig. 3a, it can be seen that the discharge curve of 15 mol% Al–$Ni(OH)_2$ becomes stable after the 11th discharge. The 11th to 40th discharge curves virtually overlap during the whole discharge duration. They only separate slightly at the end of discharge, which indicates the good cycle stability of the material. The fifth discharge curve shows a noticeable lower voltage, probably because the cathode material may have undergone some small structural changes during the first cycles. These changes may result in a rise in the redox potential or an evolution and stabilization in the ohmic drop in the composite electrode during the initial cycles. The discharge curve of high-density spherical nickel hydroxide is given in Fig. 3b. This is similar to the discharge curves of the commercial batteries. The discharge curve of 10 mol% Al–$Ni(OH)_2$ and 5 mol% Al–$Ni(OH)_2$ are shown in Fig. 3c and d, respectively. From Fig. 3c, it is observed that the 15th discharge curve begins to change significantly (note the separation of the 15th discharge curve from the 5th, 7th, 11th discharge curves after 40 min) This indicates that 10 mol% Al–$Ni(OH)_2$ fades faster than the 15 mol% Al–$Ni(OH)_2$. The 5-mol% Al–$Ni(OH)_2$ also shows faster fading as indicated by splitting of the discharge curves in Fig. 3d.

Shape differences between the discharge curves for different cathode materials as given in Fig. 3. Fig. 3a shows a stable voltage over a long duration after an initial fast decrease of voltage. This behaviour represents a perfect discharge plateau. The curves in Fig. 3b have relative less stable voltage duration compared with the curves in Fig. 3a. The voltage decreases slower than that of Fig. 3a for first part, which causes the discharge curves to appear as a quasi-plateau. As revealed by Barnard et al. [18], the β–β system has a stable potential only in the mixed phase of $Ni(OH)_2/NiOOH$ which extends from $H_{1.75}NiO_2$ to $H_{1.25}NiO_2$. Conway and Gileadi suggested that potential of charged nickel hydroxide remained constant for states of charge between 20 and 50%. The 15 mol% Al–$Ni(OH)_2$ sample overcomes this limitation and provides a longer stable working voltage. On the other hand, the α–γ system has a lower middle plateau redox potential compared in the β–β system [18]. The Al stabilized α phase has lower free energy (ΔG_f) of formation compared α phase and sustains

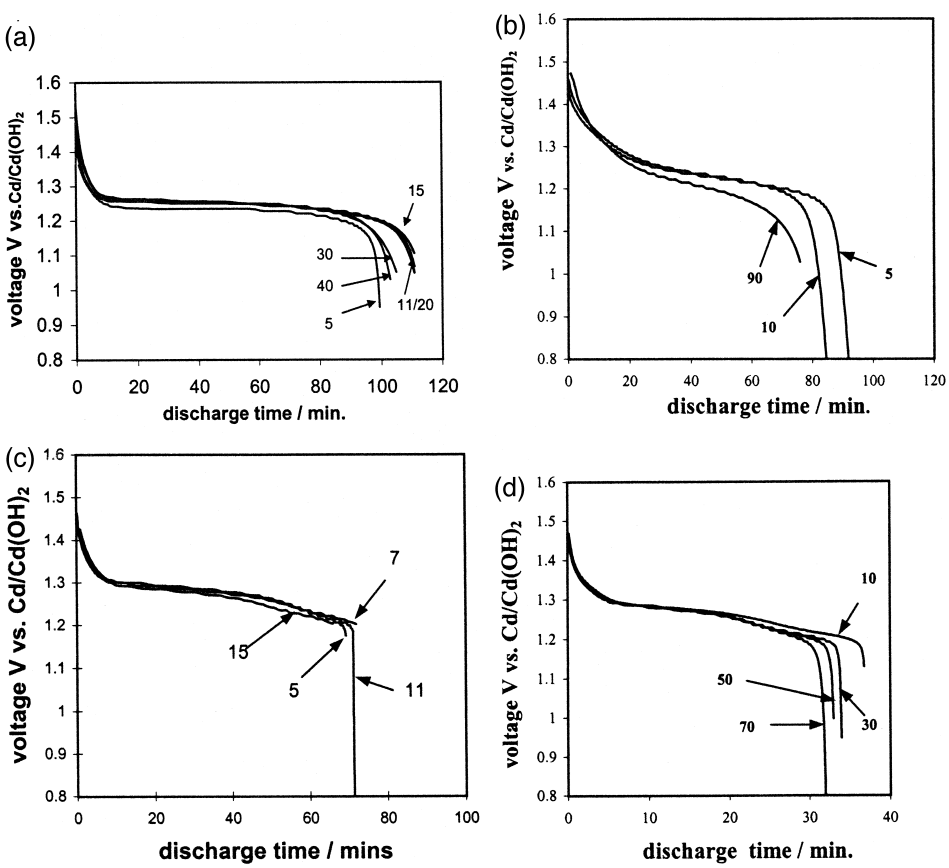

Fig. 3. Discharge curves for cells with different nickel hydroxides, discharge current: 9.4 mA, electrode area: 3.14 cm^2, (a) 15 mol% Al–$Ni(OH)_2$; (b) high-density spherical β nickel hydroxide; (c) 10 mol% Al–$Ni(OH)_2$; (d) 15 mol% Al–$Ni(OH)_2$.

a higher potential working voltage. The lower ΔG_f is the reason why the material can remain stable in strong alkali for a long time.

Similar discharge curves are shown in Fig. 3c and d. These are two quasi-plateau, which may have resulted from two different phase compositions.

3.3. Structural change and stability of cathode materials

To study the structural changes of different cathode materials, the XRD patterns of the cathode materials were examined after charge–discharge cycles. The patterns for 15 mol% Al–$Ni(OH)_2$, in a discharged state after cycles 15 and 100 and 200% overcharged state after cycle 15 are shown in Fig. 4a. The XRD pattern for 15 mol% Al–$Ni(OH)_2$ before charge–discharge cycling is also given in curve *A*. Curves *B* and *D* were obtained from cells with graphite as the conducting additive and *C* was obtained from a cell with nickel powder as the additive. From a comparison of curves *B* and *C*, it is possible to separate out the overlapping of some diffraction peaks with the peaks of the conducting additives that, otherwise, would cause some of the newly formed phases to be undetected as mentioned in Section 2. From the curves *A*, *B* and *C*, it can be seen that the lowest 2θ peaks shift to higher 2θ during the charge–discharge cycles. The 2θ values of A, B and C is 11.152, 11.561 and 11.663°, respectively, which correspond to inter-sheet distances of 7.927, 7.648, 7.581, Å, respectively. This means that the inter-sheet distance in the c-axis decreases during charge–discharge cycling. This change becomes slower during the cycling. It may be stable eventually. Also the similarity between curves *A*, *B* and *C* implies that the basic structure of 15 mol% Al–$Ni(OH)_2$ is stable except for minor changes in the lattice parameters. The diffraction peaks of curve *A* are

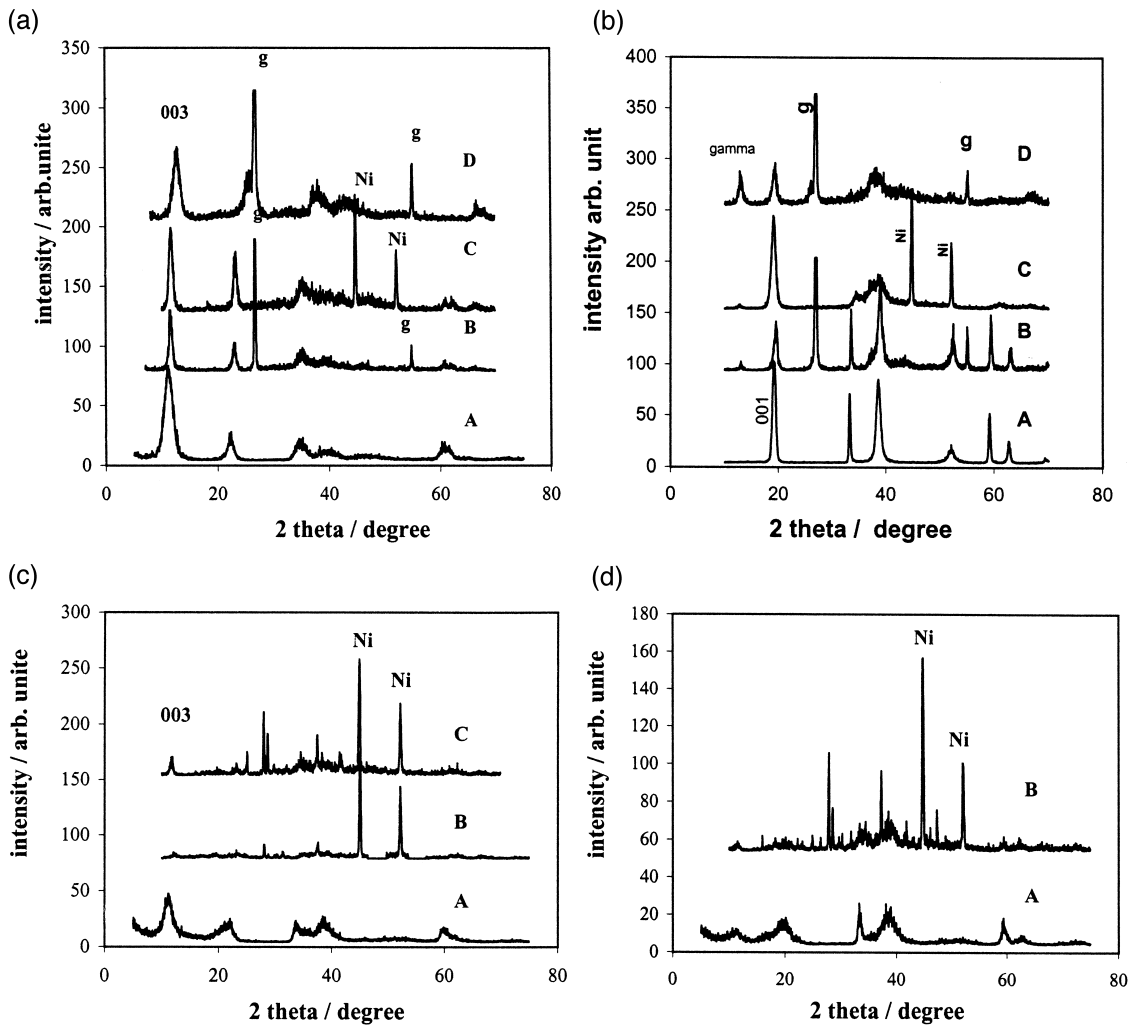

Fig. 4. XRD patterns of different nickel hydroxides after charge–discharge cycling. (a) 15 mol% Al–$Ni(OH)_2$, (A) raw material, (B) discharge state after 15th cycle; discharge to 0.9 V and 6 h — 80% overcharge in each cycle. (C) discharge state after 100th cycle; discharge to 0.9 V and 7 h — 60% overcharge in each cycle; (D) 200% overcharged state after 15 cycles as in (B). (b) high-density spherical β nickel hydroxide, (A) raw material, (B) discharge state after fifth cycle, discharge to 0.9 V, 6h — 80% overcharge in each cycle. (C) discharge state after 100 cycles, discharge to 0.9 V, 5.8 h — 60% overcharge in each cycles. (D) 200% overcharged state after 10 cycle as in (B). (c) 10 mol% Al–$Ni(OH)_2$, (A) raw material, B: discharge state after 100 cycles, discharge to 0.9 V, 4.5 h — 60% overcharge in each cycle. (C) 80% overcharge state after five cycles, 6 h — 80% overcharge in each cycle. (d) 5 mol% Al–$Ni(OH)_2$, (A) raw material, (B) discharge state after 100 cycles, discharge to 0.9 V, 4.5h — 60% overcharge in each cycle.

wider than those of curves *B* and *C*, probably because the crystallites become larger or crystallinity increases during charge–discharge cycles. However, the widths of corresponding peaks in curves *B* and *C* are nearly identical, which means that the size of crystallites or crystallinity change less against further cycling compared with the changes during the first several cycles. This may be the reason for the change in discharge voltage, as indicated before. In curve *C*, the two clear diffraction peaks of 110 and 113 at $2\theta = 60.90$, and 62.16° are noted, which may be attributed to more pure α phase being formed after 100 cycles. It is easy to understand if curve *E* in Fig. 1 is referred again, in which two relative peaks are at 60.72 and 62.16°. A consists of only one peak at 60.74°. Curve *D* is the XRD pattern of the 200% overcharged state of the 15-mol% Al–$Ni(OH)_2$. It is similar to that of γ-NiOOH. Comparing with the discharged state, the diffraction peaks shift to higher 2θ values, which means that the inter-sheet distances decrease during charging. The 003 peak of curve *D* is at a 12.76° 2θ, which translates to an inter-sheet distance of 6.934 Å, that is, 0.993 Å less than that of curve *A*. Also, the similarity of the XRD patterns between the charged and discharged states implies an iso-structural reaction during the charge–discharge process. During charging, protons de-intercalate from the inter-sheets of NiO_6 and the oxidation number of nickel increases, which results in decreased inter-sheet distances. In contrast to the β(II)–β(III) system, the Al-stabilized α–γ system consists of only a single charged phase and cannot experience a large inter-sheet distance change, even after overcharge, which is the major reason for stability and resistance to overcharge.

The structural changes of the higher-density spherical β-$Ni(OH)_2$ during charge–discharge cycling are shown in Fig. 4b. Curve *B* illustrates the structural changes of high-density spherical β-$Ni(OH)_2$ after the fifth cycle, it maintains predominantly the β structure. After 100 cycles, however, the XRD pattern of the discharged state change markedly compared with that of the original material. In curve *C*, except for the 001 peak, the other diffraction peaks are broad, which shows that the crystallinity decreases upon cycling. The100 and 101 peaks become much broader and overlap. Also, the 001 peak becomes slightly broader, which implies that the crystallites become smaller upon charge–discharge cycling. Breaking of crystallites may cause this behaviour. Curve *D* is the XRD pattern for the overcharged state. From the curve, it is seen that the overcharged state consists of β and γ-NiOOH. This agrees with the results of other workers [4]. Upon discharging, γ-NiOOH may produce the α phase. The formation of the α phase and the fading to the β phase may cause foliation and rapid fading of electrode capacity. The structural changes of 10 mol% Al–$Ni(OH)_2$ and 5 mol% Al–$Ni(OH)_2$ after charge–discharge cycling are presented in Fig. 4c and d, respectively. Complex and weak diffraction peaks are present, probably because the materials are mixed phases and fade fast to lower crystallinity after charge–discharge cycling. The lattice breaking causes 10 mol% Al–$Ni(OH)_2$ and 5 mol% Al–$Ni(OH)_2$ to have less capacity and cycle stability, as shown by their electrochemical performance.

4. Conclusions

α-phase nickel hydroxide stabilized by 15 mol% Ni substitution with Al is stable during charge–discharge cycling. The highest specific discharge capacity is 260 mA h g^{-1}, which corresponds to 1.0 electron conversion. Even after overcharge, the stabilized α phase still converts to a single γ phase nickel oxyhydroxide phase that can be discharged to the original α phase. Different from the β–β system, the Al stabilized α–γ conversion can maintain the basic crystal structure and experience small crystallographic change even in the overcharge condition. This results in high stability and resistance to overcharge. If the stabilized α nickel hydroxide is used in nickel electrode-based secondary batteries, long cycle-life and resistance to overcharge should be expected.

References

[1] S.U. Falk, A.J. Salkind, Alkaline storage Batteries, Wiley, New York, 1969.
[2] A.J. Salkind, M. Klein, Alkaline storage batteries, in: 4th edn., Kirk-Othmer Encyclopedia of Chemical Tech. Vol. 3 Wiley, New York, 1992.
[3] M. Klein, F. McLarnon, Ni–Zn batteries, in: D. Linden (Ed.), Handbook of Batteries, 2nd edn., McGraw Hill, NY, 1995, Chap. 29.
[4] H. Bode, K. Dehmelt, J. Witte, Electrochem. Acta. 11 (1966) 1079.
[5] R.S. McEwen, J. Phys. Chem. 75 (1971) 1782.
[6] P. Oliva, J. Leonardi, J.F. Laurent, C. Delmas, J.J. Braconnier, M. Figlarz, F. Fiev, A. deGuibert, J. Power Sources 8 (1982) 229.
[7] W.E. O'Grady, K.I. Pandya, K.E. Swider, D.A. Corrigan, J. Electrochem. Soc. 143 (1996) 1613.
[8] D.A. Corrigan, S.L. Knight, J. Electrochem. Soc. 136 (1989) 613.
[9] G.W.D. Briggs, W.F. Wynne-Jones, Electrochem. Acta. 7 (1962) 241.
[10] A. Delahaye-Vidal, M. Figlarz, J. Appl. Electrochem. 17 (1987) 589.
[11] C. Delmas, Y. Borthomieu, C. Faure, Solid State Ionics 32/33 (1989) 104–111.
[12] P. Vishnu Kamath, L. Mridula Dixit, A.K. Indira, V. Shukla, N. Ganesh Kumar, J. Electrochem. Soc. 141 (1994) 2956.
[13] M. Dixit, P.V. Kamath, J. Gopalakrishnan, J. Electrochem. Soc. 146 (1999) 79.
[14] W.T. Reichle, J. Catal. 94 (1985) 547.
[15] W.T. Reichle, Solid State Ionics 22 (1986) 135.
[16] T.D. Xiao, P.R. Strutt, B.H. Kear, H. Chen, Wang, Nanostructured Oxide and Hydroxide Materials and Methods of Synthesis Therefor, US Patent filed 11-18-96.
[17] P.C. Milner, U.B. Thomas, in: Advances in Electrochemistry and Electrochemical Engineer Vol. 5 Interscience, New York, 1967, p. 42.
[18] R. Barnard, C.F. Randell, F.L. Tye, J Appl. Electrochem. 10 (1980) 109–125.
[19] N. Sac-Epee, M.R. Palacin, A. Delahaye-Vidal, Y Chabre, J.M. Tarascon, J. Electrochem. Soc. 145 (1998) 1434.